Reconstruction of neutrino energy in a large water Čerenkov detector using lepton information

A.Blondel, M.Campanelli, M.Fechner

CERN-OPEN-2002-049
10/04/2002

Abstract

In this note we study the reconstruction of neutrino energy from the knowledge of the beam direction and the energy and angle of the reconstructed lepton in quasi elastic electron and muon neutrino CC interactions. As a practical example, we consider the case of a prospective CERN-Frejus experiment based on the SPL and a Super Kamiokande-like water Čerenkov detector.

1 Introduction

The aim of this work is to understand how well one can reconstruct the neutrino energy using quasi elastic neutrino-nucleus scattering. In oscillation studies, the reconstruction of the energy spectrum of the oscillated and non oscillated events can bring substantial information on oscillation parameters. So far, in the study of the low energy SPL→Frejus possible superbeam, no use has been made of this information. We assume to have a water Čerenkov detector. At these energies, quasi-elastic neutrino-nucleon scattering is the dominant interaction in the detector. We have thus neglected all other kinds of possible interactions. Only the produced lepton is above Čerenkov threshold and is therefore observed (the recoiling proton is not observed). In this study we proceed in different steps. In order to provide a cross-check of the studied algorithm, we assume at first that the detector is perfect, ie the reconstruction is infinitely accurate (no smearing of the energy and angle of the observed lepton) and there are no nuclear effects (ie no Fermi motion, no Pauli blocking and no nuclear potential well). In a second stage, we take into account all previous effects, together and separately. Resolution for a water Čerenkov detector is taken from SuperKamiokande ([4] and [5]). The description of nuclear effects is based on the Fermi Gas model (used in [14]), using the values in Ref.[9, 13] for the parameters.

2 Description of the simulation

2.1 Energy Reconstruction

We consider here the case of a neutrino beam, with an energy smaller than 2 GeV, the average event energy being approximately 350 MeV. Thus the interactions within the detector are mainly charged-current (CC) quasi elastic neutrino-neutron scattering, namely $\nu_l + n \longrightarrow l^- + p$. Considering as a first approximation that the neutron is at rest, one obtains: $m_n + E_\nu = E_p + E_l$ and $P_\nu = P_l \cos(\theta) + P_p^{\parallel}$ and $P_l \sin(\theta) = P_p^{\perp}$ (parallel and orthogonal to the neutrino's direction). These equations lead to the possibility of reconstructing neutrino energy from lepton information only:

$$E_\nu = \frac{m_n E_l + \frac{m_p^2 - m_n^2 - m_l^2}{2}}{m_n - E_l + P_l \cos(\theta)} \tag{1}$$

where θ is the angle between the outgoing lepton and the neutrino direction. This angle can be measured via the knowledge of the beam direction, and the reconstructed lepton direction in the detector.

2.2 Simulation of neutrino events

We generate $\theta^\star$ (lepton angle in the CM frame) according to the differential cross-section $\frac{d\sigma}{d\Omega}$ given in [15] and [16]. At the low energies involved in such collisions, it is necessary to include nuclear effects in the simulation. Fermi motion is described by generating neutrons with an isotropic random momentum distributed according to the density

$$W(k) = \begin{cases} \frac{3k^2}{k_f^3} \text{for } k \in [0, k_f] \\ \\ 0 \text{ for } k > k_f \end{cases}$$

with $k_F = 225$ MeV/c see Ref. [9],[16]. The event is then generated in the center of mass frame of the neutrino and the moving neutron, according to the same angular distribution, and boosted back to the lab frame. The lab frame proton momentum is then used to emulate Pauli blocking (see below). We consider a simplified description of ^{16}O nuclei: we have chosen to generate isotropic neutrons with a random momentum lower than k_F according to the previously given density; it is equally necessary to take into account the nuclear potential which affects the target nucleons. According to [7], the depth of the nuclear potential is $V = \frac{K_F^2}{2M} + E$, where M is the nucleon mass and E is the binding energy for nucleons in the outer shell ($E \approx 8$ MeV). However in this formula they take $K_F \approx 290$ MeV [1], which leads to $V \approx 50$ MeV. We substract this value from the raw value of the center of mass energy: this amounts to saying that the extraction of a proton from the potential well has a 50 MeV energy cost. It is clear that a variety of models will have to be considered in the evaluation of systematics.
Equation 1 is correct when the neutron is at rest; therefore in the presence of Fermi motion it leads to an error in then reconstruction of the neutrino energy. As pointed out in [14] and [16], Pauli blocking in the Fermi gas model can be implemented by forcing the outgoing proton to lie outside the Fermi sea. Therefore we compute $|\vec{P_\nu} + \vec{P_n} - \vec{P_l}|$, and reject the event if this quantity is smaller than k_F. This procedure suppresses low energy events, in accordance with physical intuition: at low energies the neutrino momentum is not high

[1] but the actual nucleon momentum is lower than $0.6 K_F$ in their model

enough to produce a proton which lies outside the Fermi sea, whereas at high energies the proton is almost always created outside the Fermi sea. This affects the electron spectra more severely than the muon spectra because the former start at much lower energies than the latter (lower reaction threshold and lower Čerenkov threshold).
The neutrino spectrum used in this study is generated using the tabulation given in [1]. The cross-section is obtained from a linear interpolation of the tabulation given in [13]. In the case of the SPL-Frejus beam (the CERN Superconducting Proton LINAC (SPL) will deliver 10^{23} protons-on-target in a conventional year (10^7 s)), assuming a 200kT-year exposure and considering the detector surface is 100 m^2, located 130 km away from the beam source (which is the distance between CERN and the Frejus site), we obtain the following number of events per year not considering Pauli blocking:

- 4700 CC muon events.
- 24 CC electron events.

(The small discrepancy between these values and those in [12] is due to the fact the we use interpolated values. The results in [12] are exactly reproduced if the cross-section is considered constant in each 100 MeV-wide bin).
In order to observe the correct number of events (calculated above using the exact cross-section values) in presence of Pauli blocking (which reduces the overall number due to the way we implement it), we have to rescale the spectra. These complications illustrate our relatively poor understanding of low energy neutrino-nucleus interactions.

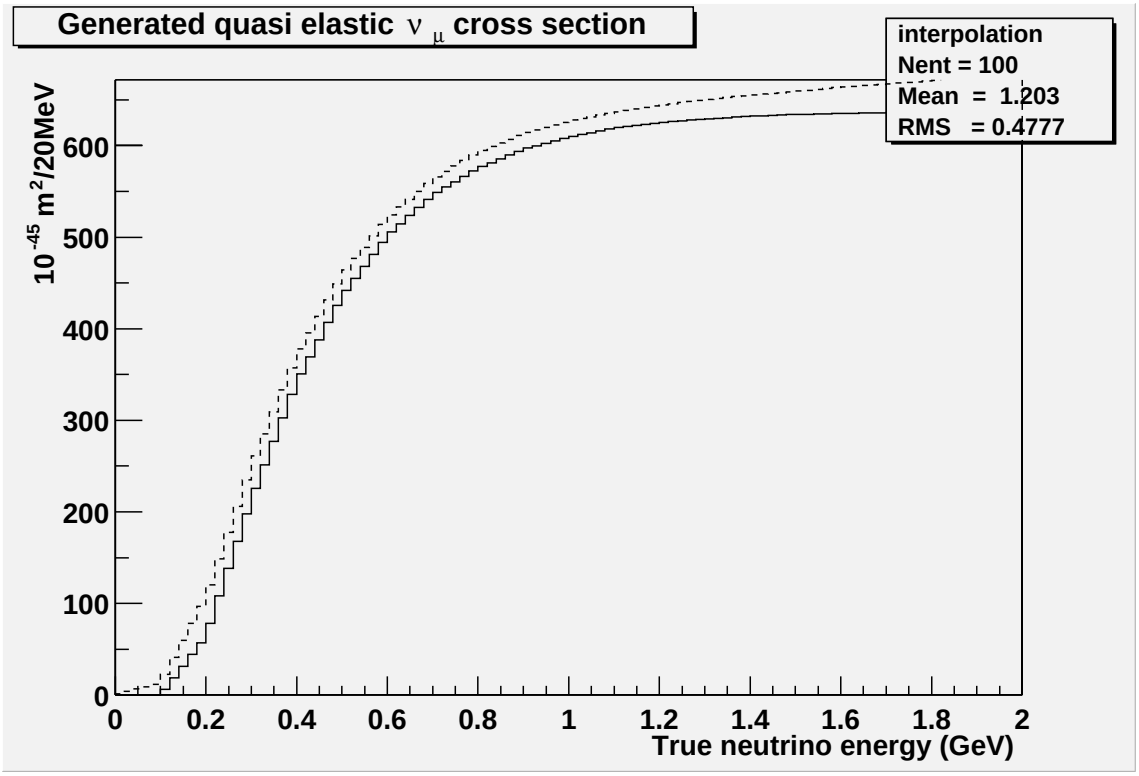

Figure 1: Plots of the cross section versus neutrino energy. The full-line is for muons while the dashed-line is for electrons.

2.3 Detector resolution

According to [4] and [5], the momentum resolution for electrons is set to $2.5\%/\sqrt{\mathrm{E(GeV)}}$ $+0.5\%$; for muons it is constant and equal to 3% in this energy range; the angular resolution is estimated to be 3 degrees, constant for electrons and muons. The momentum is smeared by generating a gaussian random number (with mean 0 and sigma equal to the computed resolution) and adding it to the reconstructed lepton momentum.
The angle is smeared using the following method: ϕ is a uniform random number chosen in $[0, 2\pi]$. A gaussian random number α of mean 0 and standard deviation 3° is generated. As resolution affects the momentum as a three-dimensionnal vector, the variation $\delta\theta$ of θ is given by $\delta\theta = \arctan(\frac{\alpha}{\theta}\cos(\phi))$. The smeared value of θ is then obtained by adding $\delta\theta$ to the raw value of θ.
These processes allow the correct description of the resolution of the water Čerenkov ring imaging detector without having to make a full description of the whole experimental apparatus.

3 Results

3.1 Results in the case of an ideal detector: testing the algorithm

In the case of the perfect detector and no nuclear effects, the reconstruction algorithm is tested and works as expected (top plots in figure 3.1): the reconstructed energy is equal to the generated energy.

3.2 Results with detector resolution (no nuclear effects)

These results show the effect of the detection using free nucleons. Switching on detector smearing introduces gaussian error on the energy reconstruction, as shown in the top plots of figures 3,4,5. These distributions appear to be gaussian, but have tails in the high-energy domain. This is believed to be the consequence of the non-linearity of the smearing procedure. (We have plotted E_ν^{rec} versus $E_\nu^{rec} - E_\nu^{true}$, for $E_\nu^{true} = 0.25$, 0.39 and 0.59 GeV). At $E_\nu^{true} = 400$MeV, the resolution is approximately 29 MeV for electrons and 20 MeV for muons.

3.3 Results with nuclear effects (no detector resolution)

In order to understand the relative importance of nuclear effects and detector resolution, we have rerun the simulation, including all nuclear effects but excluding all smearing effects. The lower-middle plots of fig. 3.1, and the middle plots in figs 3,4, 5 show the results. It can be seen that nuclear effects introduce a bias in the reconstruction process; this bias is negative for both particles, and is approximately equal to -30 MeV in this energy range. Nuclear effects also introduce an assymmetrical error in the reconstruction process as can be seen in the previous figures. This error is approximately 76 MeV for electrons and 71 MeV for muons at 400 MeV which is much greater than the error due to detector resolution.

3.4 Results including both effects (full simulation)

We have rerun the simulation, including all detector resolution effects as well as nuclear effects. The plots are shown in figures 3.1,3,4,5. It can be seen that the dominant effect in the reconstruction process is due to nuclear effects: smearing effects do not significantly

increase the spread of the reconstructed energy distribution (at 400 MeV, the increase is 4 MeV for electrons and 2 MeV for muons). It is again visible that the maximum of such distributions occurs at a lower reconstructed energy than the true energy. All those distributions are clearly assymmetrical. Figure 7 sums up all previous results, by displaying both the bias and the RMS of $E_\nu^{rec} - E_\nu^{true}$ versus E_ν^{true}.
We have also plotted the relative error of the reconstruction process, in each case (see fig. 6. It can be seen that a water Čerenkov detector is capable of reconstructing the incident neutrino energy with an error inferior to 22% in this energy range.

4 Conclusions

In this note, reconstruction of neutrino energy in a water Čerenkov detector is studied. An algorithm has been developped to this purpose, knowing the beam direction and outgoing lepton information. Nuclear effects as well as detector resolution are taken into account. The results show that it is possible to reconstruct the neutrino energy with an error smaller than 22%, for both kinds of neutrinos. We also observe that the dominant error in this reconstruction process is due to nuclear effects, which also introduce a negative bias in the reconstructed energy. The interest of such a conclusion lies in the fact that worse detector resolution can be afforded without significantly spoiling the neutrino energy measurement.

Acknowledgements

We thank M.Mezzetto for useful discussions and practical help. We are also most grateful of D.Casper's invaluable help and advice.

References

[1] M.Donega A.Blondel and S.Gilardoni. Neutrino fluxes from a conventional beam using cern spl. *NuFact Note 53*, 2000.

[2] M.Donega A.Blondel and S.Gilardoni. Study of (anti-)neutrino fluxes from a horn neutrino beam using 2.2 GeV protons. *NuFact Note 78*, 2001.

[3] A.Bohr and B.R.Mottelson. *Nuclear Structure*, chapter 2, pages 139–141. 1rst ed. edition, 1969.

[4] David Casper. private communication.

[5] The Super Kamiokande Collaboration. Measurement of a small atmospheric ν_μ/ν_e ratio. *Phys.Lett.B*, 433:9–18, 1998.

[6] C.Bleve G.Co I.DeMitri P.Bernardini D.Martello and A.Surdo. Effects of nuclear re-interactions in quasi elastic neutrino nucleus scattering. http://documents.cern.ch/archive/electronic/nucl-th/0012/0012015.pdf, December 2000.

[7] J.Ranft G.Battistoni, B.Lipari and E.Scaparone. Simulation of nuclear effects in quasi elastic and resonant neutrino interactions. *arXiv:hep-ph/9801426*, 1998.

[8] Particle Data Group. *Review of particle physics (Particle Data Book)*. Springer, 2000. Eur.Phys.J , 15 , 1-4.

[9] K.Langanke J.Engel, E.Kolbe and P.Vogel. Quasielastic neutrino scattering from oxygen and the atmospheric neutrino problem. *arXiv:nucl-th/9304017*, 1993.

[10] K.Winter, editor. *Neutrino Physics*, chapter 3: Theory of the interaction of neutrinos with matter, by L.Maiani. Cambridge University Press, 1991.

[11] M.Mezzetto. private communication.

[12] M.Mezzetto. Physics reach of super+beta beams. Talk given at NNN'02 Workshop, February 2002.

[13] P.Vogel. Neutrino nucleus scattering. *arXiv:nucl-th/9901027*, 1999.

[14] R.A.Smith and E.J.Moniz. Neutrino reactions on nuclear targets. *Nucl.Phys.B*, 43:605–622.

[15] C.H.Llewellyn Smith. Neutrino reactions at accelerator energies. *Physics Reports*, 3(5):261–379, 1972.

[16] T.K.Gaisser and J.S O'Connell. Interactions of atmospheric neutrinos in nuclei at low energy. *Phys.Rev.D*, 34(3):822–825, 1986.

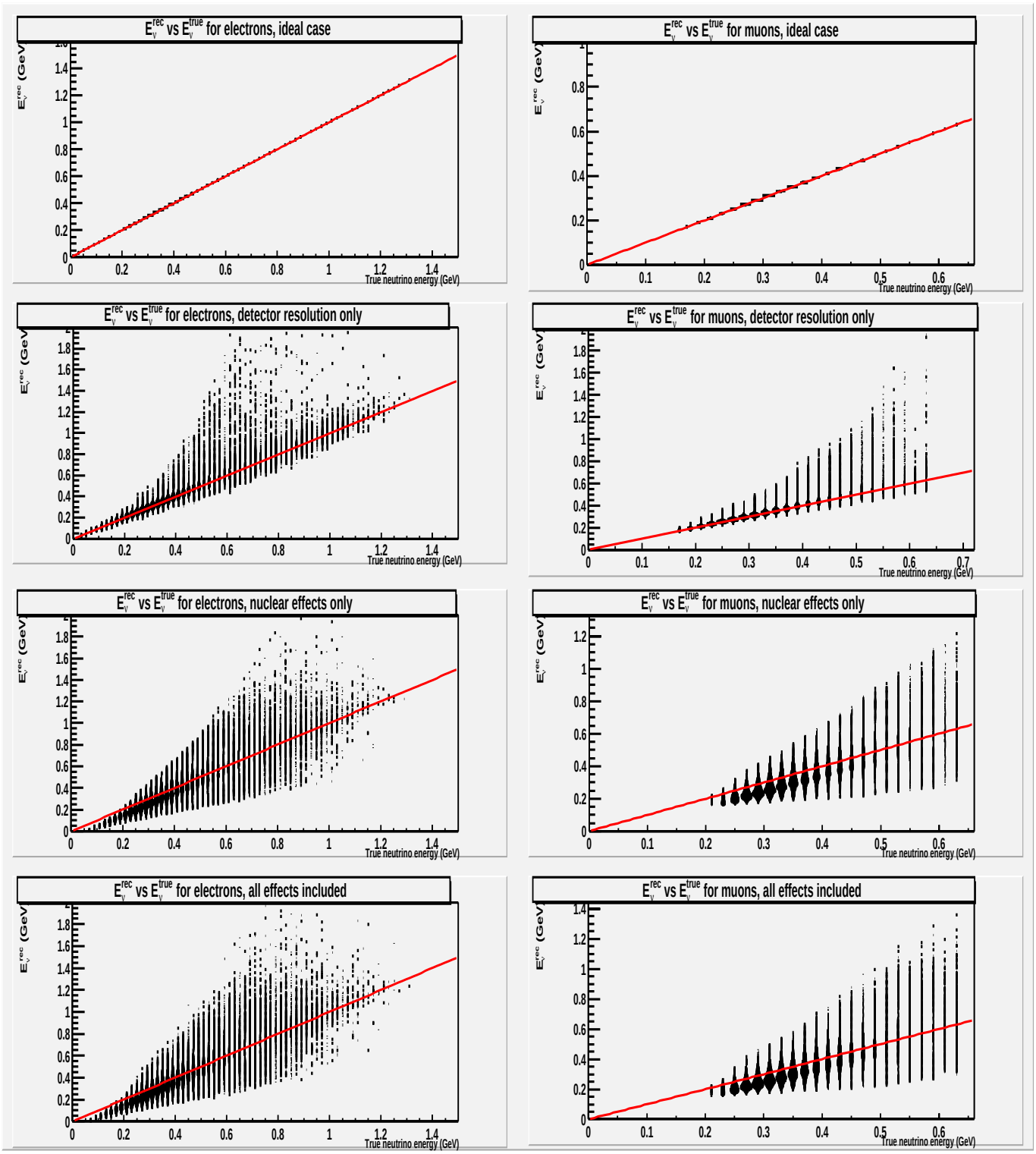

Figure 2: Reconstructed neutrino energy versus true neutrino Energy in GeV. The plots in the left-hand part of the page are for electron neutrinos, those in the right-hand part are for muon neutrinos. The top plots have been obtained in the case of a perfect detector, with no nuclear effects. The upper-middle plots show the effect of detector resolution alone (no nuclear effects: this displays detector effects on free nucleons), while the lower-middle ones show the effect of our nuclear description alone (no detector resolution). The bottom plots have been obtained with all effects turned on.

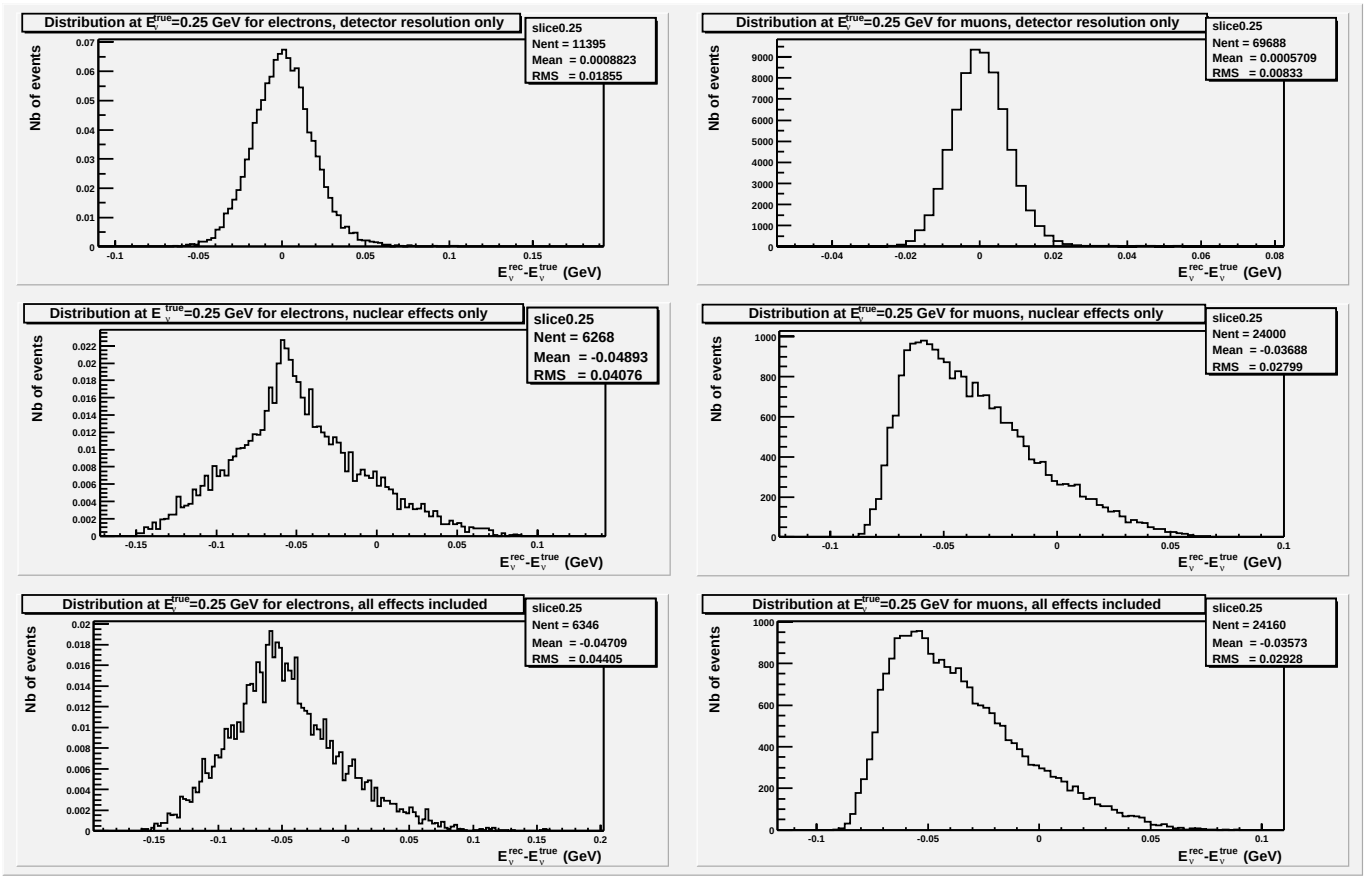

Figure 3: Plots of $E_\nu^{rec} - E_\nu^{true}$ versus E_ν^{true} ,for $E_\nu^{true} = 200\text{MeV}$. The plots in the left-hand side display electronic events, those in the right-hand side display muonic events. The top plots were obtained with detector smearing turned on, and no nuclear effects. The middle plots were obtained with nuclear effects turned on, but with no detector smearing. The bottom plots were obtained with both effects included.

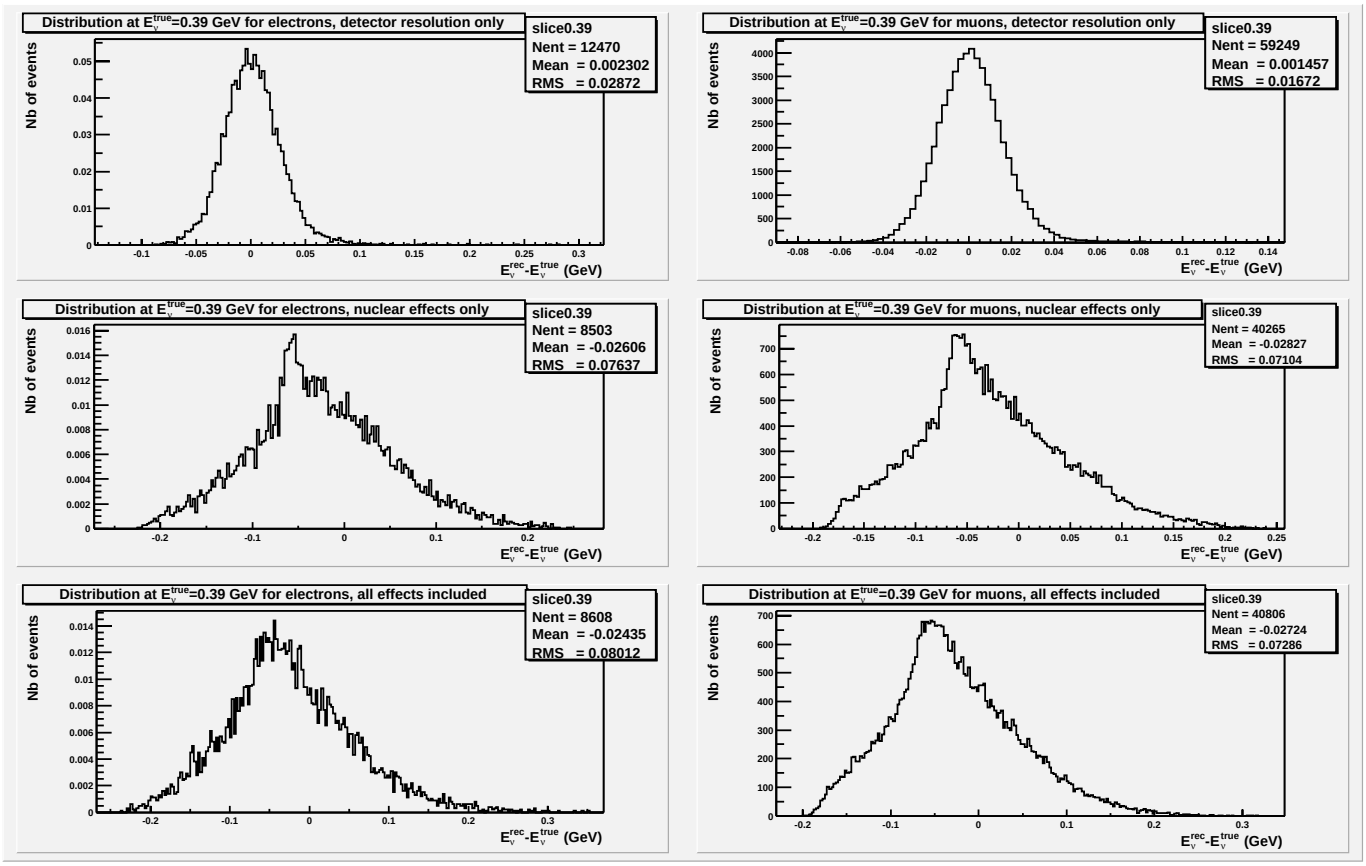

Figure 4: Plots of $E_\nu^{rec} - E_\nu^{true}$ versus E_ν^{true} ,for $E_\nu^{true} = 400$MeV. The plots in the left-hand side display electronic events, those in the right-hand side display muonic events. The top plots were obtained with detector smearing turned on, and no Fermi motion. The middle plots were obtained with Fermi motion turned on, but with no detector smearing. The bottom plots were obtained with both effects included.

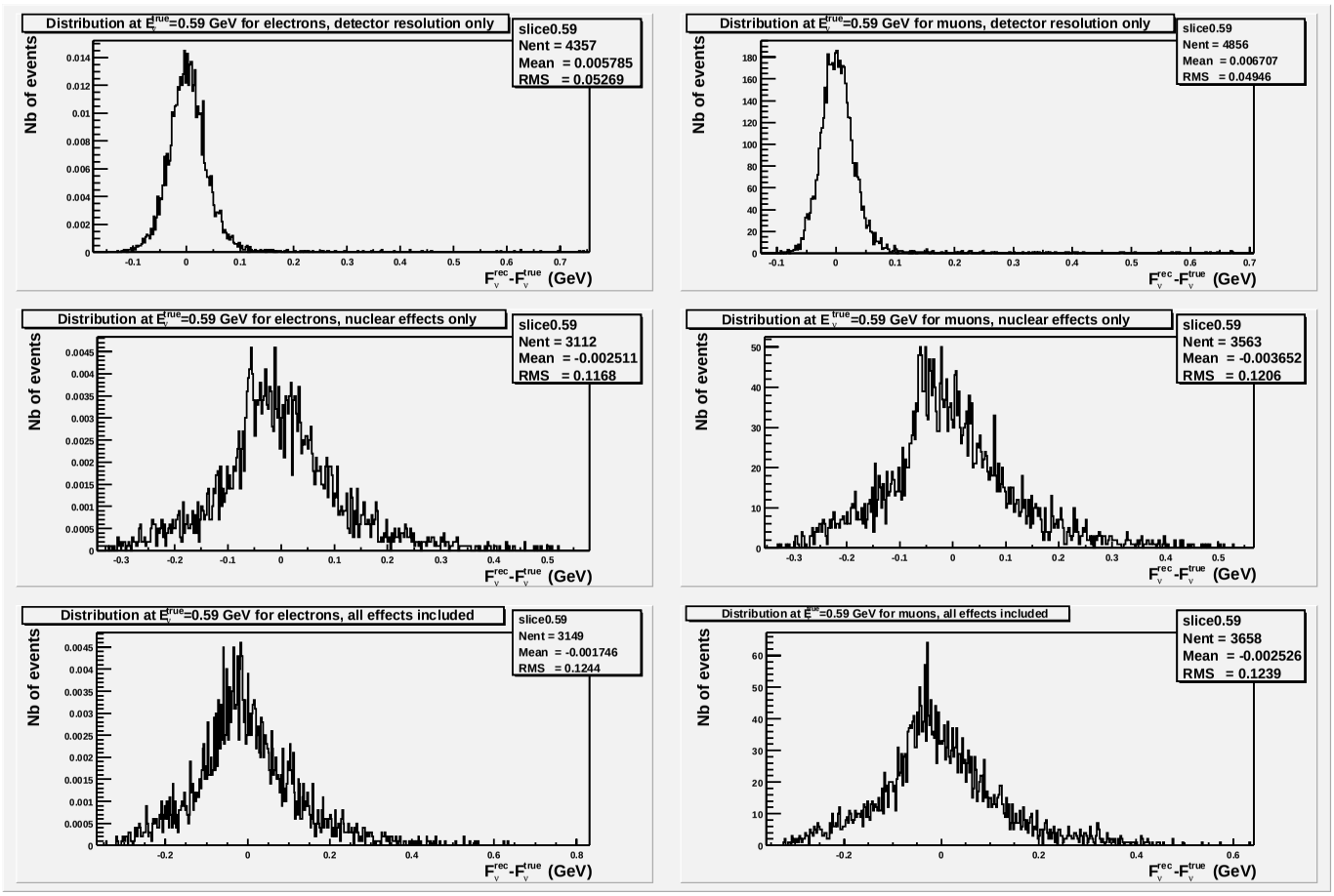

Figure 5: Plots of $E_\nu^{rec} - E_\nu^{true}$ versus E_ν^{true} ,for $E_\nu^{true} = 600\text{MeV}$. The plots in the left-hand side display electronic events, those in the right-hand side display muonic events. The top plots were obtained with detector smearing turned on, and no nuclear effects. The middle plots were obtained with nuclear effects turned on, but with no detector smearing. The bottom plots were obtained with both effects included.

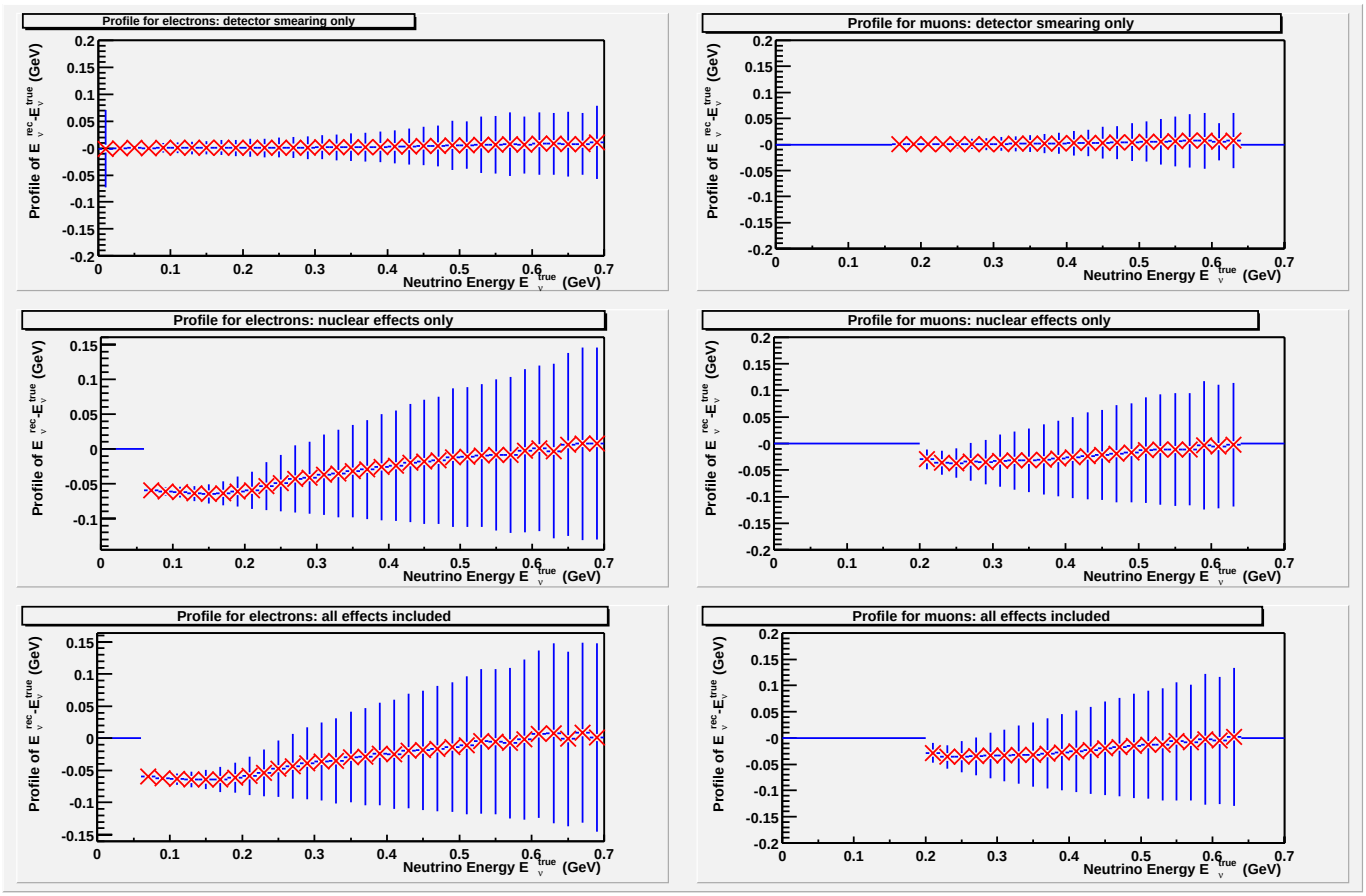

Figure 6: Profiles of $E_\nu^{rec} - E_\nu^{true}$ versus E_ν^{true}. The plots in the left-hand side display electronic events, those in the right-hand side display muonic events. The top plots were obtained with detector smearing turned on, and no nuclear effects. The middle plots were obtained with nuclear effects turned on, but with no detector smearing. The bottom plots were obtained with both effects included.

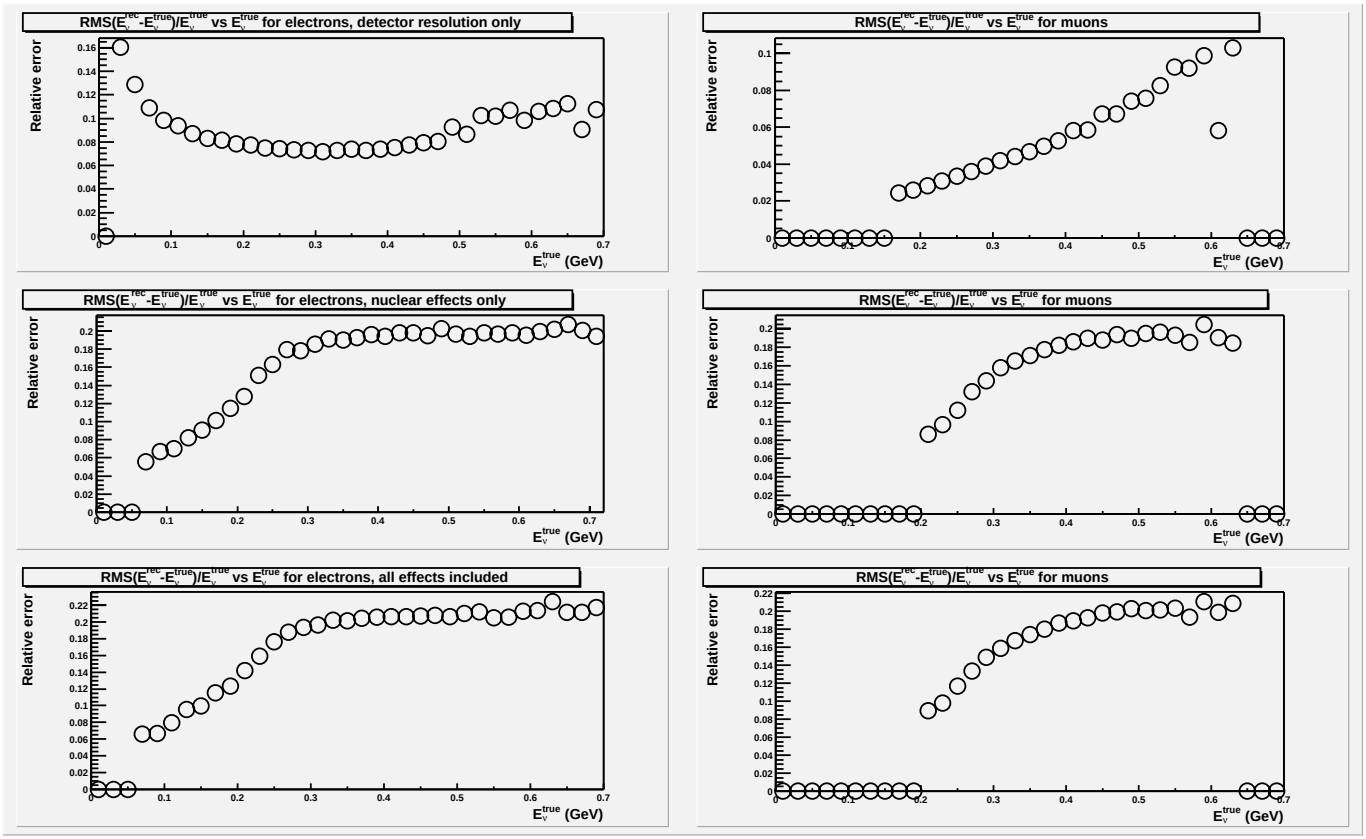

Figure 7: Relative error plots: RMS($\frac{E_\nu^{rec}-E_\nu^{true}}{E_\nu^{true}}$) versus E_ν^{true} . The plots in the left-hand side display electronic events, those in the right-hand side display muonic events. The top plots were obtained with detector smearing turned on, and no nuclear effects. The middle plots were obtained with nuclear effects turned on, but with no detector smearing. The bottom plots were obtained with both effects included.